

# R adiative T ransfer in B lack H ole S ystem s

K INWA H W U<sup>1</sup>, W ARRICK B ALL<sup>2</sup> and S T E V E N V . F U E R S T<sup>1</sup>

1. M ullard Space Science Laboratory, U niversity C ollege London,  
H olm bury St M ary, Surrey RH 5 6NT , UK
2. D epartm ent of Physics and A stronomy, U niversity C ollege London,  
G ower Street, London W C 1E 6BT , UK
3. K IPAC , Stanford U niversity, Stanford, CA 94305, U SA

## A bstract

W e present a covariant formulation for radiative transfer in curved space time and demonstrate some applications in the black-hole systems. We calculate the emission from semi-transparent accretion tori around black holes, for opacity provided by the Fe K and K lines and for opacity dominated by electron scattering. We also calculate the emission from radiative inefficient accretion flow in black holes with opacity provided by electron-positron annihilation lines. Finally we show shadows cast by accreting black holes with different spins and with different distribution of warm material around them.

## 1 G eneral R elativistic R adiative T ransfer

A black hole is characterised by a singularity and an event horizon. The presence of black holes in this universe is based on inferences, as no black hole has been observed directly. Now the question is: what does a black hole look like? Perhaps, it may be more meaningful to ask: what does an astrophysical black hole look like if we can image it, and can we see the shadow of its event horizon?

Black holes are relativistic objects. A covariant radiative transfer formulation is therefore needed to calculate the radiation from a black hole's vicinity. In the absence of scattering, the transfer equation reads

$$\frac{1}{k \cdot u} k^\mu \frac{\partial I}{\partial x^\mu} - k^\mu k^\nu \frac{\partial I}{\partial k^\nu} = \sigma_0(x; k) I + \epsilon_0(x; k) \quad (1)$$

(Lindquist 1966; Baschek et al. 1997; Fuerst and Wu 2004, 2007; Wu and Fuerst 2008), where  $k$  is the 4-momentum of the photon and  $u$  is the 4-velocity of the medium. The specific intensity  $I$ , absorption coefficient  $\sigma_0$  and emission coefficient  $\epsilon_0$  are in Lorentz invariant forms. The left side of the equation describes the radiation propagation; the right side specifies how the radiation interacts with the medium. When the velocity fields of the emitters and absorbers are given, the transfer equation can be solved along the geodesics using a ray-tracing algorithm.

Scattering deflects photons into the line-of-sight. In its presence the radiative transfer equation is an integro-differential equation. Fuerst (2005) used projection momentum tensors to decompose the transfer equation into a set of momentum equations. The first two momentum equations are

$$\begin{aligned} m J_{\mu\nu}; n^\mu + J_{\mu\nu} m^\mu + \frac{1}{\ln E} \frac{\partial}{\partial \ln E} J_{\mu\nu} \\ = [(\rho_x + \rho_{sc}) J_{\mu\nu} + S_x S_{\mu\nu} + \rho_{sc} J_{\mu\nu} u^\mu u^\nu]; \end{aligned} \quad (2)$$

$$\begin{aligned} m m_{\mu\nu} J_{\mu\nu}; n^\mu + 2 J_{\mu\nu} m^\mu + 2 \frac{\partial}{\partial \ln E} J_{\mu\nu} \\ = (\rho_x + \rho_{sc}) J_{\mu\nu} m^\mu m^\nu + S_x S_{\mu\nu} + \rho_{sc} J_{\mu\nu} u^\mu u^\nu + \frac{1}{10} n^\mu n^\nu \end{aligned} \quad (3)$$

respectively, where  $\rho$  is the density of the medium,  $\rho_x$  is the absorption cross section,  $\rho_{sc}$  is the electron scattering cross section,  $S_x$  is the source function,  $n$  is the photon directional unit vector ( $n \cdot n = 1$ ),  $E = k \cdot u$ ,  $m^\mu = n^\mu + u^\mu = k^\mu/E$ , and  $\rho_{sc} = u^\mu n^\mu$ ;  $n^\mu + n^\mu u^\mu$ ;  $u^\mu$ . (Here, we assume that electron scattering is the prime scattering process.) The  $j$ -th order specific intensity is

$$I_j(x; k) = J_{\mu_1 \mu_2 \dots \mu_j} m^{\mu_1} m^{\mu_2} \dots m^{\mu_j} \quad (4)$$

(Fuerst 2005; Wu et al. 2006). The momentum equations are not closed. However, they would converge rapidly for certain choices of momentum functions. In practical calculations, using a truncated set of low order moments is usually sufficient.

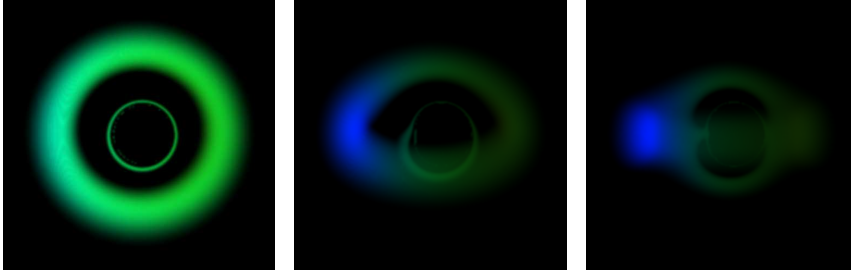


Figure 1: Surface brightness of a semi-transparent accretion torus around a Kerr black hole ( $a = 0.998$ ), viewed at inclinations of  $15^\circ$ ,  $60^\circ$  and  $85^\circ$  (left to right). The opacity is due to the Fe K $\alpha$  and K $\beta$  lines. The brightness is normalised, with all tori having equal maximum pixel brightness.

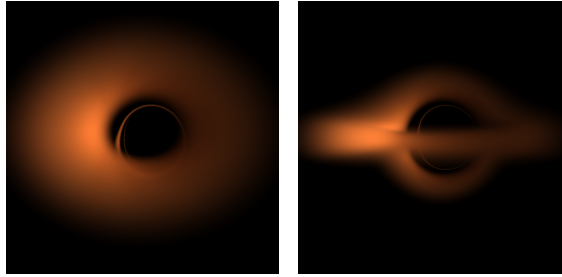


Figure 2: Surface brightness of a semi-transparent electron scattering accretion torus around a Kerr black hole ( $a = 0.998$ ), viewed at inclinations of  $45^\circ$  (left) and  $85^\circ$  (right). Brightness normalisation is the same as that in Figure 1.

## 2 Imaging Black Holes

Figure 1 and 2 show the images of accretion tori around Kerr black holes. The opacities are provided by the Fe K $\alpha$  and K $\beta$  lines and by electron scattering respectively in the two cases. For the case in Figure 1, the non-scattering formulation (Eq. 1) is used in the calculations; for the case in Figure 2, the moment radiative transfer formulation (Eq. 2, 3 and 4) is used. The velocity field and density distribution in the tori are determined using an empirical velocity law gauged by magneto-rotational instability simulations of accretion disks (see Fuerst and Wu 2004, 2007). The brightness

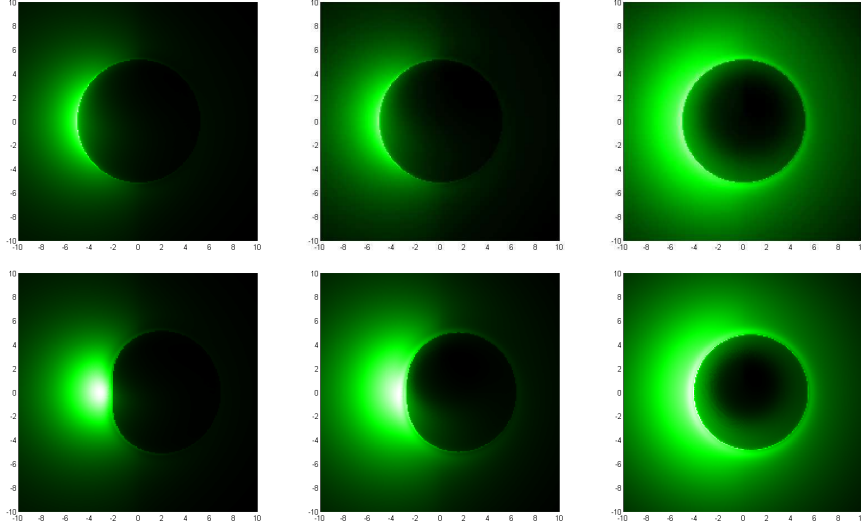


Figure 3: Intensity images of emission lines from vertically Gaussian-distributed hot plasmas around a Schwarzschild black hole (top row) and a Kerr black hole with  $a = 0.998$  (bottom row). The density distribution takes the form:  $n(r; z) / z^{3/2} \exp(-z^2/H^2)$ . The viewing inclinations are 75, 45 and 15 (left to right columns). The opacity is provided by the electron-positron annihilation line.

distributions of the tori in the images reflect the combined effects of gravitational and kinematic frequency shifts, Doppler boosting, and line-of-sight path length variations caused by gravitational lensing and frame dragging.

Figure 3 shows the emission images of electron-positron annihilation lines from hot accretion flows. We adopt a vertically Gaussian density distribution  $n(r; z) / z^{3/2} \exp(-z^2/H^2)$ , where the scale height  $H$  is determined by the thermal sound speed and the rotational Keplerian angular velocity (see Ball 2008 for details). This density distribution is appropriate for hot radiative inefficient accretion flows. A similar density distribution was used in the black-hole shadowing calculations by Huang et al. (2007). The emission images of the Schwarzschild and Kerr black holes are distinguishable with the differences more obvious for larger viewing inclination angles.

Figure 4 shows the shadows in a starry background sky cast by black holes with a Bondi-Hoyle accretion flows, i.e. the density distribution of material  $n(r) / r^{3/2}$ . The emissions from the stars are gravitationally

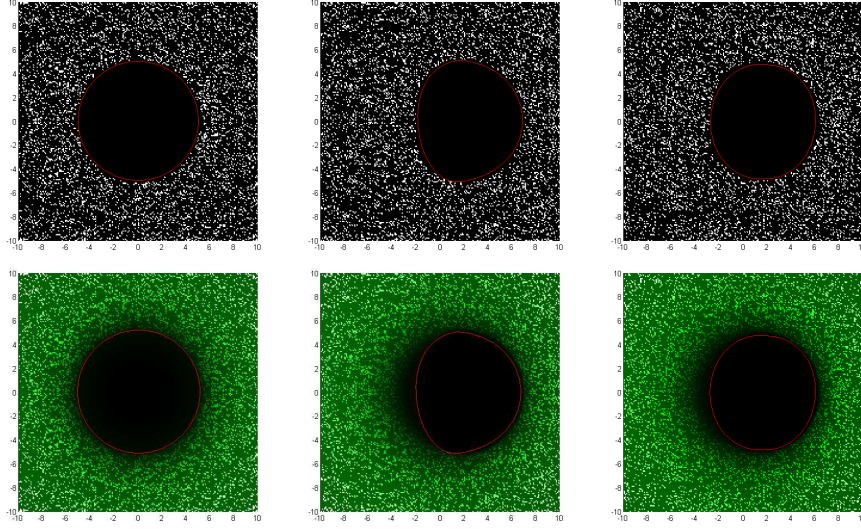


Figure 4: Shadows of a background sky cast by Schwarzschild black holes (left column), and Kerr black holes with  $a = 0.998$  viewed at inclination of  $90^\circ$  (middle column) and  $45^\circ$  (right column). The optical depth is provided by a spherical inflow of warm accreting gas with a temperature  $T = 5 \times 10^5$  K. The density distribution of the gas takes the form  $n(r) \propto r^{-3/2}$ . The line-of-sight opacity  $\tau = 0$  for the black holes in the top row, and the mean line-of-sight opacity  $\tau = 5$  for the black holes in the bottom row. The stars in the background sky are randomly generated and have the same brightness. The red line denotes the locations of geodesics crossing the event horizon.

lensed, but the stellar emissions have no frequency shifts because the stars are at infinite distances. However, the stars appear to distribute unevenly in the images and the centroid of the shadow appears to shift when the black hole rotates. These phenomena happen for two reasons. The first is due to 'geometrical effect', which is caused by rotational frame dragging of the black hole. This can be seen easily when comparing the images in the top panels. The shadow is not circular and the centroid shifts if the black hole rotates. The distortion depends on both the black-hole spin and the viewing inclinations. The second is due to 'optical depth effect'. Gravitational lensing and frame dragging have different effects on the lines-of-sight for different impact parameters and for different photon incidence with respect to the black hole's spin axis (in the case of Kerr black holes).

The integrated optical depths are not the same along different lines-of-sight. In the bottom panels of Figure 4, the emissions of the stars at the left side of the event horizon are more strongly absorbed than the emissions of the stars at the right side.

## Acknowledgements

We thank Colin Young and Susan Young for reading through this manuscript and for comments.

## References

- [1] Ball, W. H. : 2008, M Sc Thesis, University College London, UK .
- [2] Baschek, B. , Ertmer, G. V. , von Waldenfels, W. and Wehrse, R. : 1997, A & A , 317, 630.
- [3] Fuerst, S. V. : 2005, PhD Thesis, University College London, UK .
- [4] Fuerst, S. V. and Wu, K. : 2004, A & A , 424, 733.
- [5] Fuerst, S. V. and Wu, K. : 2007, A & A , 474, 55.
- [6] Huang, L. , Cai, M. , Shen, Z.-Q. and Yuan, F. : 2007, MNRAS, 379, 833.
- [7] Lindquist, R. : 1966, Ann. Phys., 37, 487.
- [8] Wu, K. and Fuerst, S. V. : 2008, AIPC, 968, 411.
- [9] Wu, K. , Fuerst, S. V. , Lee, K.-G. and Branduardi-Raymont, G. : 2006, ChJAS, 6 (Supplement 1), 205.

## DISCUSSION

THOMAS SCHWEIZER : Is it possible to measure the spin of a black hole and the last stable orbit by looking at the emission lines?

KINWAH WU : In principle, yes. In practice, it is more complicated to deduce the black-hole parameters from the emission lines because of degeneracy. The emission line profiles are not uniquely determined by the location of the last stable orbit of particles, and hence the black hole's spin.